nature physics

Article

https://doi.org/10.1038/s41567-023-02029-z

Interdependent superconducting networks

Received: 5 August 2022

Accepted: 20 March 2023

Published online: 01 May 2023

Check for updates

I. Bonamassa[1,2,3] ✉, B. Gross[1,3], M. Laav[1,3], I. Volotsenko[1], A. Frydman[1] & S. Havlin[1]

Cascades are self-amplifying processes triggered by feedback mechanisms that may cause a substantial part of a macroscopic system to change its phase in response to a relatively small local event. The theoretical background for these phenomena is rich and interdisciplinary, with interdependent networks providing a versatile framework to study their multiscale evolution. However, laboratory experiments aimed at validating this ever-growing volume of predictions have not been accomplished, mostly because of the lack of a physical mechanism that realizes interdependent couplings. Here we demonstrate an experimental realization of an interdependent system as a multilayer network of two disordered superconductors separated by an electric insulating film. We show that Joule heating effects due to large driving currents act as dependency links between the superconducting layers, igniting overheating cascades via adaptive and heterogeneous back-and-forth electrothermal feedback. We characterize the phase diagram of mutual superconductive transitions and spontaneous microscopic critical processes that physically realize interdependent percolation and generalize it beyond structural dismantling. This work establishes a laboratory manifestation of the theory of interdependent systems, enabling experimental studies to control and to further develop the multiscale phenomena of complex interdependent materials.

Catastrophic events such as power-grid outages[1,2] or regime shifts in urban infrastructures[3–5] and other complex systems[6–10] are often the aftermath of cascading processes[11,12] spreading within and across multiple layers of the network. Interdependent network theory[13,14] has provided a framework to study these multiscale phenomena, translating the mechanisms fuelling the propagation of avalanches into the interplay between two qualitatively different types of couplings: connectivity links[15] that characterize the interactions between nodes within layers and dependency links that model functional interactions (for example, positive feedback) of nodes between networks. Despite many theoretical efforts made in applying this so-called two-interaction scheme to processes as diverse as percolation[16–19], dynamics[20,21] and transport[22], developing physics-laboratory realizations of interdependent systems has remained an elusive challenge, meaning that experimental studies to scrutinize and develop the interdisciplinary volume of models and predictions collected so far have not been possible.

In this Article we present the experimental and theoretical characterization of the first physical interdependent material based on a multilayer network composed of two disordered superconductors separated by a thermally conducting electrical insulator. We model this as thermally coupled networks of Josephson junctions, and elucidate the mutual percolation processes that underlie the discontinuous onset and fall of global phase coherence observed in our experiments. We disclose fundamental features of interdependent interactions related to their spontaneous emergence, the strength of their action and the suppressive effect they have on the process of functional revival. These results establish a laboratory-controlled benchmark of the theories

[1]Department of Physics, Bar-Ilan University, Ramat-Gan, Israel. [2]Department of Network and Data Science, CEU, Vienna, Austria. [3]These authors contributed equally: I. Bonamassa, B. Gross, M. Laav. ✉e-mail: bonamassai@ceu.edu

https://doi.org/10.1038/s41567-023-02029-z

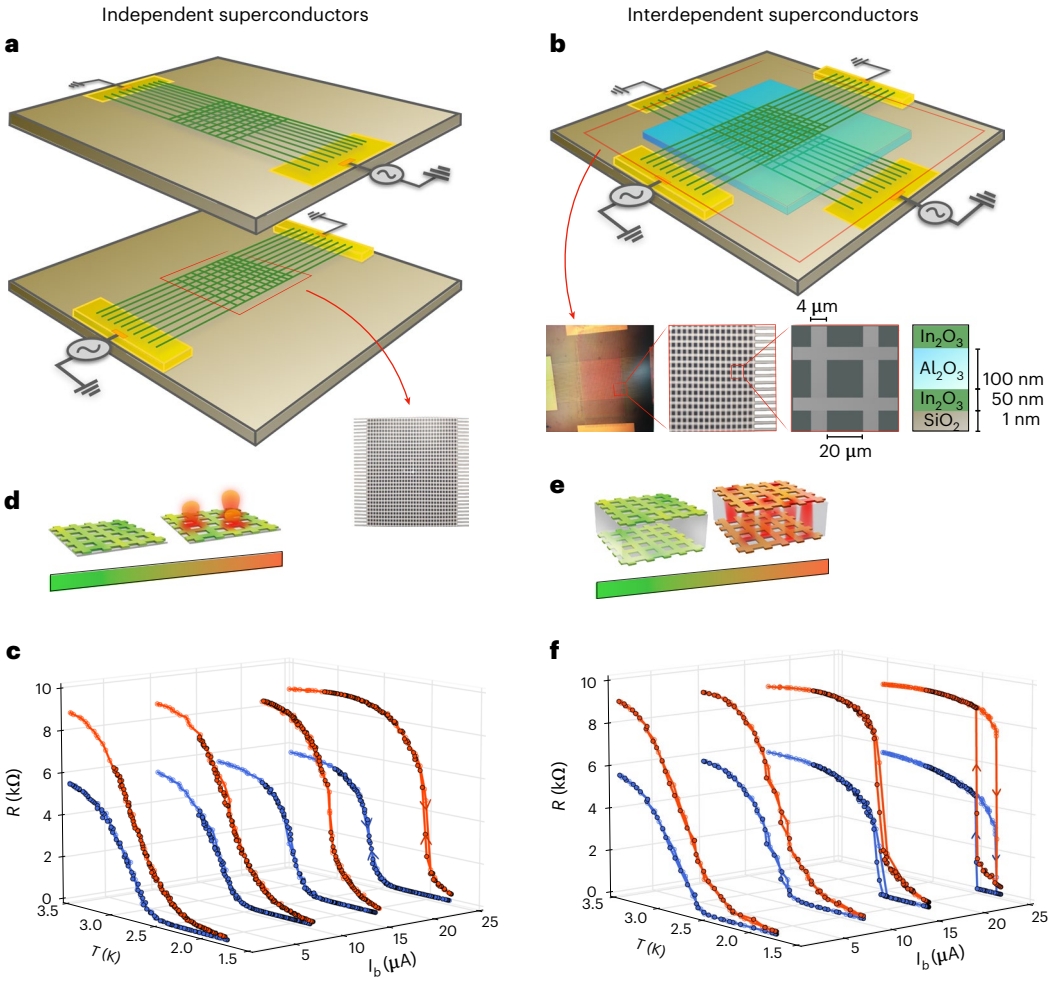

Fig. 1 | Design and experimental setup of thermally interdependent superconducting networks. a, Schematic representation and scanning electron micrograph (enlarged inset) of the isolated layers, each involving a 2D lattice of disordered superconductors (a:InO films on SiO_2 substrates, see Methods for details). The edges of each network are connected to Au/Ti contacts. **b**, Design of the interdependent superconducting material, with bottom and top layers (green grids) separated by a thermally conducting insulating film (Al_2O_3). Inset, scanning electron micrograph of the interdependent sample and characterization of the physical dimensions of the layers. **c**, Experimental sheet resistances measured in the isolated top (red) and bottom (blue) layers under identical driving currents at zero magnetic field, for increasing (filled symbols) and decreasing (empty symbols) values of the cryostat temperature T (see the arrows along the curves at $I_b = 24$ μA). Both layers undergo continuous SN transitions at different bulk critical temperatures. **d**, Illustration describing the emergence of local normal-metal (N) hotspots at the SN transition of single layers for large enough driving currents. **e**, In the interdependent setup, local hotspots thermally intertwine the SC states of superposed junctions, physically realizing the cross-layer dependency links. **f**, Sheet resistance measured in the interdependent superconducting networks for the same set of driving currents displayed in Fig. 1c. For $I_b \gtrsim 15$ μA the layers become thermally locked in their bulk critical temperatures and undergo unconventional mutual first-order SN transitions.

of interdependent systems and enhance our understanding of their complexity beyond modelling.

Experimental results

Figure 1 shows the schematic design of our multilayer material composed of two disordered superconductors[23] in two configurations: independent networks (Fig. 1a) and thermally interdependent networks (Fig. 1b), where cross-layer couplings set in through an electrically insulating film with good thermal conductivity (Al_2O_3). Each layer is composed (full details about the sample preparation are given in Methods) of an electron-beam evaporated amorphous indium oxide (a:InO) film, which is a disordered superconductor characterized by a broad superconducting transition with a bulk critical temperature, $T_c \approx 3$ K, determined by the onset of global phase coherence.

The experimental results presented in Fig. 1c,f can be summarized as follows. When measured independently and under identical conditions, as illustrated schematically in Fig. 1a, each layer undergoes a continuous and broad superconductor–normal (SN) phase transition[24,25] at some finite bulk critical threshold, T_c, whose value depends on the disorder of the sample and on the driving current, I_b, flowing through it. Since the layers have different levels of disorder—each segment has a different critical current and temperature—they exhibit different values of T_c. The broad SN transitions become sharper for increasing values of I_b but they always remain continuous and non-hysteretic (Fig. 1c). On the other hand, when a similar sufficiently large I_b flows simultaneously in both layers, as illustrated in Fig. 1b, thermal couplings set in between the networks and their SN transitions become mutually abrupt and hysteretic (Fig. 1f). Furthermore, we find that the mutual superconducting (SC) to normal-metal (N) transitions are dominated by the high disordered network (having lower T_c), while the mutual N-to-SC (NS) jumps are governed instead by the resistive behaviour of the low disordered array (having higher T_c).

Two-interaction mechanism

The unconventional discontinuous SC transitions reported in the experiments can be understood within the framework of

interdependent networks[13,26]. Each independent layer realizes a typical instance of the disorder via its characteristic distribution of critical temperatures $\{T^{c}_{ij}\}_{i,j\leq N}$ and currents $\{I^{c}_{ij}\}_{i,j\leq N}$, with N being the number of nodes in the two-dimensional (2D) lattices, which control the SN activation of single junctions due to the Josephson effect. It follows that the bulk critical temperature T_c of these disordered media[27] corresponds to the threshold (at constant I_b) where SC clusters continuously percolate[28–30]. The experimental independent sheet resistances displayed in Fig. 1c confirm the continuous and reversible nature of the SN transition in the isolated SC networks at two independent values of T_c over the range of driving currents tested.

We now consider the interdependent scheme (Fig. 1b). Slightly above their independent critical temperatures, single layers lack the percolation of SC paths, hosting, instead, the flow of dissipative currents. Single junctions switching to the N state therefore become localized hotspots (Fig. 1d) randomly distributed across each array, whose dissipated heat depends on how much current flows through them[31]. The Al_2O_3 medium (Fig. 1b, inset) couples thermally the two networks by mediating the heat from the hotspots between the layers while inhibiting the tunnelling of electrons. In this configuration, physical dependency links spontaneously emerge between the layers in the form of adaptive thermal couplings sustained by Joule dissipation[32,33], which thermally intertwine the SC states of superposed junctions (Fig. 1e). More concretely, we assume that once a junction a_{ij} in layer A switches into metal (Fig. 2a), it overheats its superposed junctions in layer B, thus raising the vulnerability of the latter junctions to exceed their critical temperature. This outcome causes a redistribution of the currents in layer B that can activate other junctions, for example $b_{\ell m}$, as they cross their critical currents, creating more hotspots that heat back their counterparts around $a_{\ell m}$ in layer A.

This positive electrothermal runaway, that physically realizes the two-interaction interplay theorized in interdependent percolation[13], ignites avalanches of switching junctions whose non-local growth across the layers can encompass a large fraction of the system's size (Methods), causing the mutual first-order SN transitions displayed in Fig. 1f. In particular, heating the networks from low temperatures realizes the propagation of damage created by cascading failures (here, N states) in interdependent percolation, yielding the mutual fragmentation of the SC phases in both layers. On the other hand, when cooling the system from its mutual N phase, thermal interdependence defers the formation of global phase coherence to temperatures below the T_c of each isolated array, producing areas of hysteresis. In this cooling process, the dissipating hotspots sustain the mutual N phase by suppressing the merging of SC clusters, realizing a mechanism opposite to cascading failure that is analogous to spanning-cluster-avoiding percolation[34]. In fact, we provide support based on our theoretical model below (Fig. 2a) that compact SC clusters become dense at low T until they suddenly merge into a giant percolating SC component (see also Supplementary Figs. 3 and 4 and Supplementary Videos 1 and 2), yielding an abrupt onset of global coherence in both arrays that nicely reproduces the mutual NS transitions found in the experiments (Fig. 1f). We stress that qualitatively similar results are found by assuming a global thermal coupling between the layers instead of a local one between superposed junctions (see equation (3) and details therein). Moreover, the effect of the lattice structure of our experiment is qualitatively negligible for the general problem of the two-interaction mechanism in interdependent networks. In fact, because of the random distribution of the critical currents and temperatures of each bond, the current flowing through each of the two arrays follows diluted backbones with strongly dissimilar profiles (see Supplementary Videos 1 and 2). Such heterogeneity and asymmetry, together with the interweaving of the current redistribution due to the thermal couplings between the layers (Fig. 2a), result in a degree of complexity qualitatively analogous to the one observed in many real-world systems (Discussion).

Theoretical modelling

To microscopically characterize the electrothermal feedback underlying the mutual SN phase transitions observed in the experiments, we develop a framework (Fig. 2a) of thermally interdependent disordered 2D lattices of resistively shunted Josephson junctions (RSJJs). In this model (see Methods for details), the state (SC, intermediate, N) of a given bond, (i,j), is set via a Josephson current–voltage (I–V) characteristic (Fig. 2b) defined by the junction's critical current I^{c}_{ij} and its normal-state resistance R^{n}_{ij}, whose values depend on the local temperature, T_{ij}, reached around it. We describe the latter by generalizing the de Gennes relation[35] to a local form given by

$$I^{c}_{ij}(T_{ij}) = I^{c}_{ij}(0)\left(1 - T_{ij}/T^{c}_{ij}\right)^{2}, \tag{1}$$

where $I^{c}_{ij}(0)$ is the zero-T critical current of the junction (i,j) and T^{c}_{ij} is its activation temperature, whose values (caption, Fig. 2c) are extrapolated from the experimental data (Methods). To control the degree of disorder in the lattices, we consider a normal distribution with zero mean and standard deviation σ, in terms of which we generate the zero-T critical currents of each junction, their critical temperatures T_c and the N state resistances R^{n}_{ij}.

When the driving currents $I_{b,A}$ and $I_{b,B}$ injected in the two arrays are kept constant, an increase (decrease) of the cryostat temperature, T, controls the SN phase transitions of each layer since it reduces (increases) the critical current of single junctions as in equation (1). This response generally depends on the presence of Joule heating effects, which can intertwine the states of the overlapping junctions. If thermal couplings are absent, then the local temperatures T^{A}_{ij} and T^{B}_{ij} in the arrays coincide with T and the distributions of the critical currents vary homogeneously with the temperature. In this case, local phase perturbations are damped out and produce rapid transients during which the current optimally redistributes its flow over new isoresistive paths. By solving numerically[36] the Kirchhoff equations (Methods) of the isolated RSJJ networks, we find that this redistribution of the currents yields only continuous SN transitions, with resistive curves (Fig. 2c) whose broadness and threshold depend on the degree of disorder of each array (Supplementary Fig. 1).

This scenario changes when the RSJJ networks are thermally interdependent. In this case, the states of two overlapping junctions, for example a_{ij} in layer A and b_{ij} in layer B, interact with each other through their local temperatures. To include this mutual overheating effect, we consider the dissipation $\mathcal{P}_{ij,t} = R_{ij,t}I^{2}_{ij,t}$ of the junctions at the t-th stage of the overheating cascade, where $R_{ij,t}$ is the resistive state of the junction (Methods, equation (M1)), so that the local temperatures T^{A}_{ij} and T^{B}_{ij} at the t-th overheating cascade are iteratively given by

$$T^{\mu}_{ij,t} = T + \frac{\tau_p}{\tau_e}\gamma^{-1}\mathcal{P}^{\mu'}_{ij,t-1}. \tag{2}$$

Here, γ (W K^{-1}) is the thermal conductance of the coupling medium and $\mu' \neq \mu$, with $\mu, \mu' = A, B$. In equation (2), the ratio τ_p/τ_e between the two relevant time scales (τ_p for phonons and τ_e for electrons) characterizing the heat rate transferred through the coupling medium and the one emitted by Joule dissipation (see Methods for details) have values that generally depend on the geometry of the sample as well as on the physical properties of the superconducting materials. To support equation (2) we stress that, in our experiment, the thickness of the Al_2O_3 layer is roughly two orders of magnitude (Fig. 1b, inset) smaller then the lattice spacing within each array and its thermal conductivity[37] is about 50 times larger then the SiO_2 (ref. 38) substrate (respectively, 10 W m^{-1} K^{-1} versus 0.2 W m^{-1} K^{-1}). This indicates (Methods) that the junctions are weakly thermally coupled within the layers so that equation (2) is valid, at least to leading orders. Under this condition, the iterative two-interaction interplay set between the layers by equation

https://doi.org/10.1038/s41567-023-02029-z

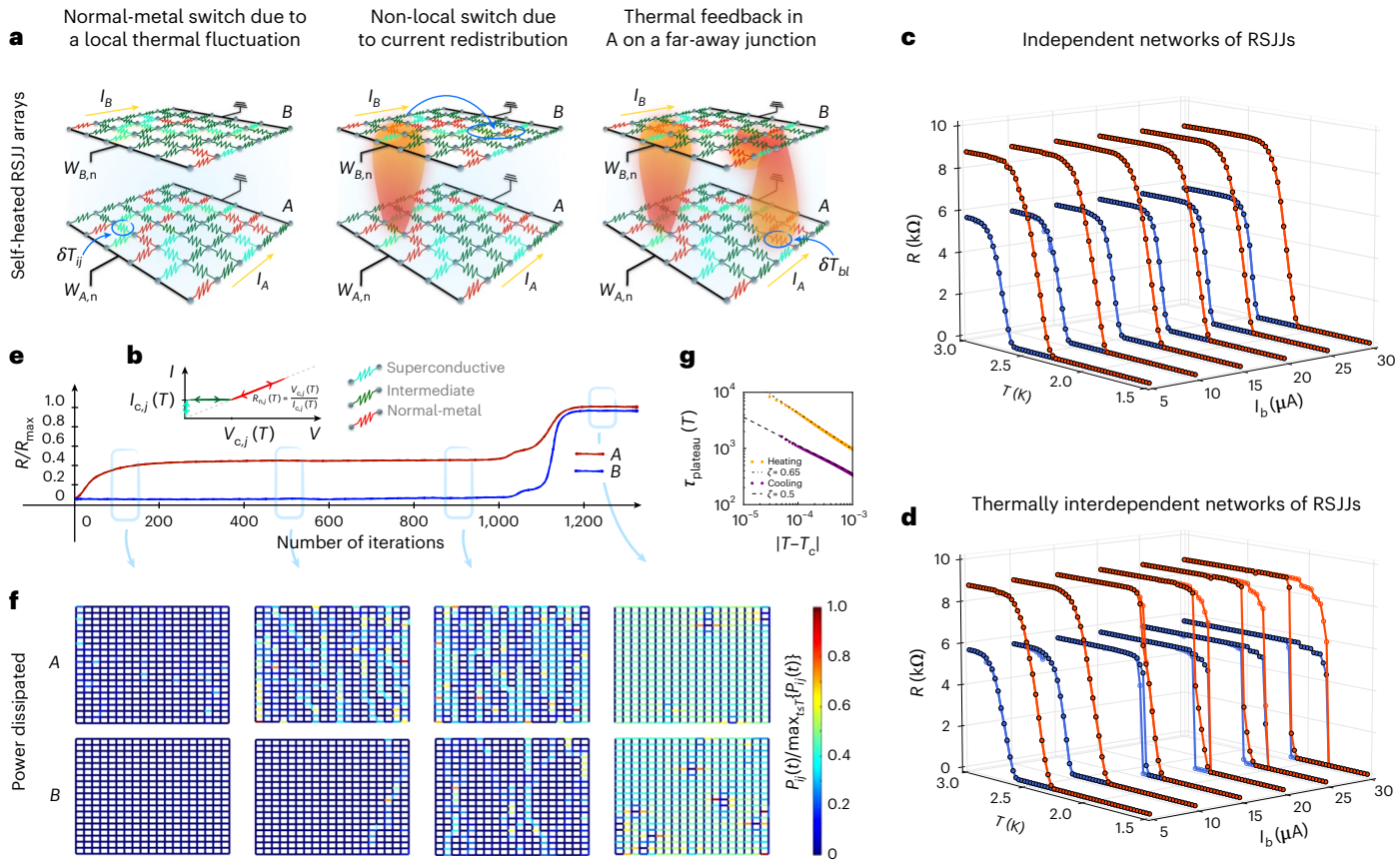

Fig. 2 | Thermally interdependent networks of RSJJs. a, Illustration of the electrothermal runaway caused by the local hotspots and the redistribution of the currents when transitioning from the mutual SC phase to the mutual N phase. A description of the cascading stages in the heating (SC-to-N) and cooling (N-to-SC) processes is given in the text. **b**, Josephson *I*–*V* characteristic adopted to model the switching of single junctions between their electronic states (details about the RSJJ model are given in Methods). **c**, Continuous SN transitions in the global resistances of two thermally decoupled arrays with 1,860 junctions with mean critical thresholds $I^c_{0,A} = 52\ \mu A$ and $T^A_c = 2.4$ K (top layer, red symbols), $I^c_{0,B} = 76\ \mu A$ and $T^B_c = 2.7$ K (bottom layer, blue symbols), with variances $\sigma_A = 0.06$ (high disordered layer) and $\sigma_B = 0.04$ (low disorder layer). We adopt the normal resistive factors section $\rho_A = 1.24$ and $\rho_B = 0.77$, matching the experimental ratio $R_A/R_B \approx 1.61$. **d**, Mutual resistive transitions in interdependent RSJJ networks obtained by solving numerically the thermally coupled Kirchhoff equations (Methods, equations (M2) and (M3)) set by the two-interaction interplay between equation (1) and equation (2) with $\gamma = 8 \times 10^{-3}\ W\ K^{-1}$ and $\tau_p/\tau_e \approx 1.7 \times 10^6$ (Methods). The remaining parameters are identical to those in **c**. **e**, Evolution of the marginally stable mutual SC phase for $I_b = 24\ \mu A$ slightly above the heating first-order SN threshold, $T_{c,>} = 2.08$ K, displaying the emergence of a long-lived plateau with nearly constant resistances. **f**, Stroboscopic snapshots of the power dissipated by single junctions during the heating plateau in **e**; notice the propagation of local hotspots (dark red links) between the layers *A* and *B* due to the overheating cascades. **g**, Scaling of the metastable lifetime as a function of the temperature, $\tau(T)$, at $I_b = 24\ \mu A$ of the heating (orange) and cooling (purple) plateau close to the heating threshold ($T_{c,>} = 2.08$ K) and to the cooling one ($T_{c,<} = 1.88$ K), respectively. Notice the two scaling exponents hinting at the different growth processes (see the main text for details) that underlie the two jumps of the abrupt transition (Supplementary Fig. 4).

(1) and equation (2) yields an adaptive and heterogeneous response of the critical currents to local thermal fluctuations that describes mathematically the electrothermal runaway effect triggered by cross-layer interdependent couplings.

Mutual transitions and microscopic kinetics

To study the system of interdependent superconductors, we solve numerically the thermally coupled Kirchhoff equations (Methods, equations (M1)–(M3)) set by the process described above for disordered lattices whose physical properties (caption, Fig. 2c,d) match those in the experiments. During each stage in the cascade of overheatings, we compute the current, electronic state and the power dissipated by each junction in order to track their spatio-temporal evolution (Supplementary Figs. 2 and 3 and Supplementary Videos 1 and 2).

Macroscopically, we find that with currents $I_{b,A}, I_{b,B} \geq 15\ \mu A$ the system enters a regime of mutual first-order SN transitions (Fig. 2d) accompanied by different relaxation processes. Figure 2e,f shows, in particular, the bulk resistances of the layers and the local power dissipated by single junctions when letting the system evolve from the mutual SC phase to the mutual N phase at a temperature *T* slightly above the first-order SC-to-N threshold, $T_{c,>}$. As displayed in Fig. 2e, above $T_{c,>}$ the mutual SC phase develops a long-lived plateau relaxation characterized by nearly constant resistances, whose duration (Fig. 2g) $\tau \propto (T - T_{c,>})^{-\zeta}$ with exponent $\zeta \approx 0.65$ diverges at $T_{c,>}$ (Supplementary Fig. 4c,d). In the cooling direction, the evolution from the mutual N phase to the mutual SC phase exhibits an analogous metastable regime (Supplementary Fig. 4a,b) whose duration (Fig. 2g) diverges at the N-to-SC threshold, $T_{c,<}$, as $\tau \propto (T_{c,<} - T)^{-\zeta}$, with exponent $\zeta \approx 0.5$.

Microscopically, the different critical exponents (Fig. 2g) of the metastable lifetime can be adopted as proxies for the underlying cascading processes[39], indicating that the SC nuclei grow faster than the N nuclei. During the heating plateau, this can be explained in terms of the pinning of the interfaces between SC clusters and N nuclei, which halts the branching of the latter, while the smaller (in fact, mean-field[40]) exponent of the cooling plateau hints at the sudden merging of thermally suppressed SC clusters. The critical nature of these microscopic

https://doi.org/10.1038/s41567-023-02029-z

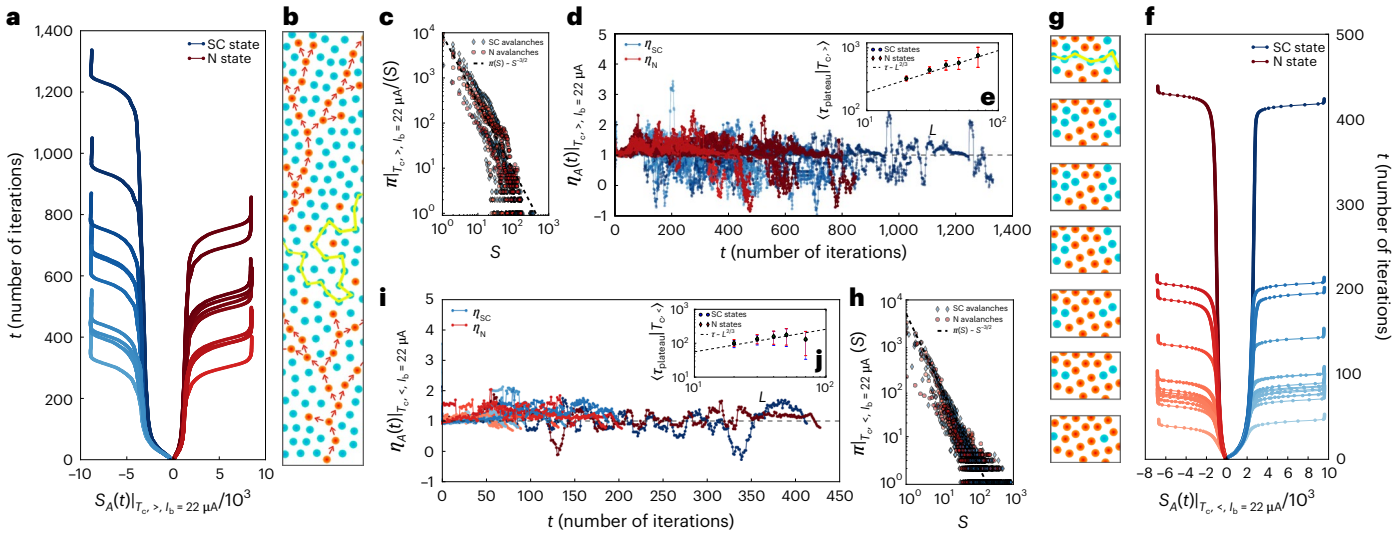

Fig. 3 | Microscopic kinetics and their lifetime at the first-order transition thresholds. a, Plateau relaxation of the avalanche size for the N state (red symbols) and the SC state (blue symbols) switching junctions measured in layer A at the SC-to-N threshold (lattice linear size $L = 70$, driving current $I_b = 22$ μA, $T = T_{c,>} = 2.08$ K). Time steps have units of successful switches (meaning that zero variations of $S(t)$ are traced out from the time series); notice that, while N states are stable at $T_{c,>}$, SC states switch unstably to the intermediate state (Fig. 2b and Supplementary Fig. 5a). **b**, Illustration of the evolution of the N-cascading trees (red symbols), branching through the junctions of the interdependent system and progressively hindering the formation of SC paths (yellow curve). **c**, N/SC-state avalanche size distribution, $\pi(S)$, at $T_{c,<}$ reported in lattices of linear size $L = 20, 30, 40, 50, 70$ over a total of 2,000 samples. **d**, Evolution of the branching factor, $\eta(t)$, for the SC/N state avalanches for 10 samples of linear size $L = 70$. While $\eta_N(t) \approx 1$ (N nuclei are critical), the SC branching factor is often subcritical; this is because its kinetics are strongly coupled with the neutral ($\eta_{IN}(t) \approx 0$) intermediate state (Supplementary Fig. 5a–d). **e**, Scaling of the average lifetime of the critical branching process at $T_{c,>}$ with the lattice linear size, L. Both N state and SC state processes follow the interdependent percolation[41] scaling $\langle\tau\rangle \propto L^{2/3}$. Error bars correspond to the standard deviation. **f**, Plateau relaxation of the avalanche size analogous to **a** here measured at the N-to-SC transition threshold, $T_{c,<} = 1.88$ K; notice the symmetric evolution of the SC/N states (see also Supplementary Fig. 5e for the role of intermediate states). **g**, Illustration of the avoiding cluster-merging process underlying the balanced nucleation of SC states (blue symbols) out of the N phase at $T_{c,<}$. **h**–**j**, Same as in **c**–**e**, respectively, for $T_{c,<} = 1.88$ K.

dynamics manifests itself in the evolution of the cascading trees generated by state-switching junctions (Fig. 3). At criticality, the avalanche size $S(t)$, which is the number of junctions cascading to the SC/N state at time t, develops a long-lived plateau during which its relative growth is a zero fraction of the system size. However, while at $T_{c,<}$ the SC phase nucleates symmetrically out of the N phase (Fig. 3f)—indicating a balanced process—at $T_{c,>}$ the evolution becomes asymmetric, reflecting the slower growth of the N nuclei (see Fig. 3a and details in the caption). The convergence of the branching factor, $\eta(t) \equiv S(t+1)/S(t)$, to $\eta_c = 1$ shown in Fig. 3d demonstrates that, at $T_{c,>}$, N nuclei spontaneously undergo a critical branching process (Fig. 3b) yielding an average lifetime $\langle\tau\rangle \propto L^{2/3}$ (Fig. 3e) and an N avalanche distribution $\pi(S) \propto S^{-3/2}$ (Fig. 3c) whose scaling nicely agrees with what is expected from interdependent percolation[41]. We find that also the symmetric birth–death process underlying the N-to-SC transition (Fig. 3f) undergoes a balanced critical branching or pruning of the SC/N-cascading trees (Fig. 3i) featuring the same scaling exponents describing the typical length (Fig. 3j) and the avalanche distribution (Fig. 3h) observed at the SC-to-N transition. Despite the different nature of the two microscopic kinetics—percolating cascades at $T_{c,>}$ (Fig. 3b) versus avoiding cluster merging[34] at $T_{c,<}$ (Fig. 3g)—their critical exponents indicate that both processes belong to the mean-field universality class of self-organized branching[42].

Mean-field solution

To further corroborate our findings, we develop an analytical mean-field solution of the thermally interdependent Kirchhoff equations under the two-interaction interplay set by equation (1) and equation (2). We build our mean-field solution on the Halperin–Nelson (HN) formula[43] $R_{HN}(T) = R_0 \exp\{-\beta(T - T_c(I_b))^{-1/2}\}$ —where R_0, β and $T_c(I_b) = T_{c,0} - \omega I_b$ are material parameters (caption, Fig. 4a)—which characterizes the resistance of a 2D superconductor slightly above its continuous SN transition. We advance a global-coupling hypothesis (see Methods for details on its validity) by adopting an all-to-all network of thermal dependency couplings between the layers so that the RSJJ arrays interact through their collective phases. This is done by replacing the local quantities in equation (2) by their global counterparts, which coarse grains the system of $4L(L-1)$ local temperatures, where L is the linear size of the lattices, into two global ones. Since the length of dependency links is random (and of the order of $\mathcal{O}(L)$), the global overheating at the t-th stage of the cascade on layer μ due to the power dissipated by layer μ' can be computed via the HN resistance of μ' at the effective temperature induced by μ on μ' at the previous stage, $t-1$, and so forth in a recursive fashion. We can then represent the evolution of overheating cascades via the recursion sequence of adaptive global temperatures:

$$T_{\mathrm{eff},t}^{\mu\leftarrow\mu'} = T + \gamma R_{\mathrm{HN}}^{\mu'}(T_{\mathrm{eff},t-1}^{\mu'\leftarrow\mu}) I_{\mathrm{b},\mu'}^2, \quad t = 1, 2, \ldots \tag{3}$$

for $\mu' \neq \mu$ and $\mu, \mu' = A, B$, with the initial seed $T_{\mathrm{eff},0}^{A\leftarrow B} \equiv T$. In the limit $t \to \infty$, the fixed points of equation (3) yield a system of self-consistent equations for the mutual bulk resistances

$$\begin{cases} R_{\mathrm{HN}}^{A}(T) = R_0^{A} \mathrm{e}^{-\beta_A/\sqrt{T - T_c^A(I_b^A) - \gamma R_{\mathrm{HN}}^{B}(T)}}, \\ R_{\mathrm{HN}}^{B}(T) = R_0^{B} \mathrm{e}^{-\beta_B/\sqrt{T - T_c^B(I_b^B) - \gamma R_{\mathrm{HN}}^{A}(T)}}, \end{cases} \tag{4}$$

that can be solved numerically for suitable choices of the material-dependent parameters (caption, Fig. 4).

We find that the mean-field theory agrees with the numerical results (Fig. 4a) and correctly captures the phenomenology of mutual SN phase transitions observed in the experiments within the accessible

https://doi.org/10.1038/s41567-023-02029-z

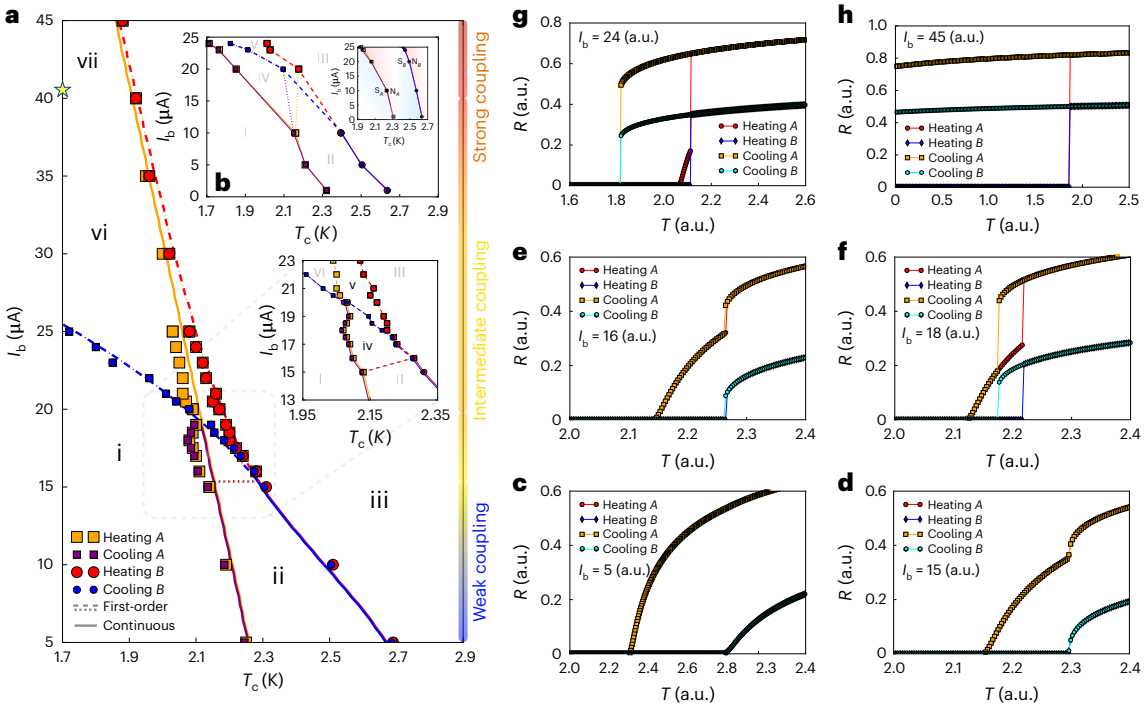

Fig. 4 | Mutual phase diagram showing theory versus experiments. **a**, Theoretical thresholds (symbols) characterizing the mutual transition thresholds in the globally interdependent Kirchhoff equations versus the analytical thresholds (curves) obtained via the interdependent HN resistances, equation (4). To solve the latter, the parameters R_0, β, ω, $T_{c,0}$ and γ (measured in arbitrary units (a.u.)) have been extracted by best-fitting R_{HN} to the numerical resistive curves of the two layers, taken independently, yielding $\beta_A = 0.40$, $\beta_B = 0.65$, $T^A_{c,0} = 2.30$, $T^B_{c,0} = 2.75$, $\omega = 10^{-2}$ and $\gamma = 4 \times 10^{-3}$; we set $R^A_0 = 1$ and $R^B_0 = 0.65$, matching the experimental ratio (caption, Fig. 2c). Inset, mutual stability: (i) mutual SC phase, meaning both *A* and *B* are stable superconductors; (ii) and (iv) *A* is a stable metal and *B* is a stable superconductor; (iii) mutual N phase, meaning both *A* and *B* are stable metals. Mutual metastability: (v) *A*-partial N and *B*-SC with the mutual N phase; (vi) and (vii) mutual N phase with mutual SC phase. Phases (iv) and (vii) differ from, respectively, phases (ii) and (vi) in their mutual transitions (see plots **c**–**h**). **b**, Experimental phase diagram extracted from the resistive curves displayed in Fig. 1f. Inset, decoupled thresholds describing the continuous SN transitions in Fig. 1c. **c**–**h**, Analytical mutual transitions at increasing interdependence strengths. Weak couplings, **c** and **d**: *A* and *B* undergo nearly independent continuous SN transitions until a cusp forms in layer *B*. Moderate couplings, **e** and **f**: *A* undergoes a two-step transition, with a continuous step from a SC phase to a partial N phase and a first-order jump to the fully N phase. Strong couplings, **g** and **h**: the partial N branch of *A* becomes metastable (red symbols) until the continuous SN threshold of layer *A* merges with its first-order jump (star symbol, Fig. 4a). Above this point, the system is purely metastable (**h**) below the bulk SC melting threshold, $T_{c,>}$, in its mutual N phase and mutual SC phase.

range of parameters (see also Supplementary Figs. 6 and 7). Depending on the values of the driving currents, we identify three main coupling regimes of increasing strengths (blue-to-red colour bar, Fig. 4a): (i) weak interdependence ($I_b \lesssim 17$), where both layers undergo continuous SN transitions (Fig. 4c,d); (ii) moderate interdependence ($17 \lesssim I_b \lesssim 40$), where two-step (continuous and first-order) transitions are observed (Fig. 4e–g); (iii) strong interdependence ($I_b \gtrsim 40$) where the system undergoes only mutual first-order SN transitions (Fig. 4h). In particular, in the intermediate regime, the continuous SN transition of layer *A*—meaning the one having the lowest bulk critical temperature—is reversible only for $I_b \lesssim 20$ (orange and red symbols, Fig. 4e,f) and it is always followed by a mutual first-order jump to the full N phase. For $I_b \gtrsim 20$, layer *A* enters a marginally stable partial N phase (red symbols, Fig. 4g and orange full line in Fig. 4a) whose threshold rapidly converges to the bulk SN heating one (dashed red curve, Fig. 4a) when I_b is increased. Instead, when cooling the system from its mutual full N phase, for $I_b \gtrsim 20$ both layers undergo coupled first-order NS (meaning N-to-SC) phase transitions whose thresholds (blue dashed curve, Fig. 4a) rapidly decrease for increasing currents. In particular, when $I_b \gtrsim 40$ (star symbol, Fig. 4a) the partial N branch vanishes and the two layers become fully thermally interdependent (see also Supplementary Fig. 6). In this regime, the mean-field theory predicts a zero-temperature mutual metal ground state that coexists with the mutual SC one (phase vii, Fig. 4a) in a thermally bistable electronic state. A full classification of the mutual phases in the system (Fig. 4a, inset) is given in the caption to Fig. 4a.

Discussion

Over the last decade, the lack of experimental realizations of interdependent systems has contrained our understanding of their complexity within the realm of mathematical modelling. The system of thermally coupled superconductors we introduced here grounds the theory of interdependent networks to the physical laboratory, allowing further study in a systematic way. For example, instead of being thermal, dependency links may emerge as magnetic, capacitive or inductive feedbacks in other physical systems—for example, coupled Berezinsky–Kosterlitz–Thouless vortices between two layers of 2D magnets[44,45]—whose experimental realization would foster the development of further interdependent materials embodying the two-interaction paradigm. We notice that, although the networks adopted in this work are inherently random and their current flow is asymmetric and heterogeneous (as discussed above), our experiment raises the challenge of fabricating disorder-controlled multilayer materials that more visibly replicate the structural and functional disorder of previously studied interdependent systems by employing lithographic techniques to further control the disorder of superconducting material. Moreover, from a more applied perspective, the discontinuity of the SN transition in coupled networks demonstrated in this work may provide an

opportunity to design innovative technologies, such as ultra-sensitive sensors[46] or multistack memory devices[47], that exploit the spontaneous emergence of mutual macroscopic phases due to the back-and-forth cascade of microscopic perturbations.

Online content

Any methods, additional references, Nature Portfolio reporting summaries, source data, extended data, supplementary information, acknowledgements, peer review information; details of author contributions and competing interests; and statements of data and code availability are available at https://doi.org/10.1038/s41567-023-02029-z.

References

1. Yang, Y., Nishikawa, T. & Motter, A. E. Small vulnerable sets determine large network cascades in power grids. *Science* **358**, eaan3184 (2017).
2. Schäfer, B., Witthaut, D., Timme, M. & Latora, V. Dynamically induced cascading failures in power grids. *Nat. Commun.* **9**, 1975 (2018).
3. Rinaldi, S. M., Peerenboom, J. P. & Kelly, T. K. Identifying, understanding, and analyzing critical infrastructure interdependencies. *IEEE Control Syst.* **21**, 11–25 (2001).
4. Rosato, V. et al. Modelling interdependent infrastructures using interacting dynamical models. *Int. J. Crit. Infrastruct.* **4**, 63–79 (2008).
5. Hokstad, P., Utne, I. B. & Vatn, J. *Risk and Interdependencies in Critical Infrastructures* (Springer, 2012).
6. Haldane, A. G. & May, R. M. Systemic risk in banking ecosystems. *Nature* **469**, 351–355 (2011).
7. Pocock, M. J., Evans, D. M. & Memmott, J. The robustness and restoration of a network of ecological networks. *Science* **335**, 973–977 (2012).
8. Helbing, D. Globally networked risks and how to respond. *Nature* **497**, 51–59 (2013).
9. Rocha, J. C., Peterson, G., Bodin, Ö. & Levin, S. Cascading regime shifts within and across scales. *Science* **362**, 1379–1383 (2018).
10. Scheffer, M. *Critical Transitions in Nature and Society*, Vol. 16 (Princeton Univ. Press, 2020).
11. Borge-Holthoefer, J., Banos, R. A., González-Bailón, S. & Moreno, Y. Cascading behaviour in complex socio-technical networks. *J. Complex Netw.* **1**, 3–24 (2013).
12. Morone, F. & Makse, H. A. Influence maximization in complex networks through optimal percolation. *Nature* **524**, 65–68 (2015).
13. Buldyrev, S. V., Parshani, R., Paul, G., Stanley, H. E. & Havlin, S. Catastrophic cascade of failures in interdependent networks. *Nature* **464**, 1025–1028 (2010).
14. Bianconi, G. *Multilayer Networks: Structure and Function* (Oxford Univ. Press, 2018).
15. Barabási, A.-L. *Network Science* (Cambridge Univ. Press, 2016).
16. Baxter, G. J., Dorogovtsev, S. N., Goltsev, A. V. & Mendes, J. F. F. Avalanche collapse of interdependent networks. *Phys. Rev. Lett.* **109**, 248701 (2012).
17. Bashan, A., Berezin, Y., Buldyrev, S. V. & Havlin, S. The extreme vulnerability of interdependent spatially embedded networks. *Nat. Phys.* **9**, 667–672 (2013).
18. Radicchi, F. Percolation in real interdependent networks. *Nat. Phys.* **11**, 597–602 (2015).
19. Klosik, D. F., Grimbs, A., Bornholdt, S. & Hütt, M.-T. The interdependent network of gene regulation and metabolism is robust where it needs to be. *Nat. Commun.* **8**, 534 (2017).
20. Nicosia, V., Skardal, P. S., Arenas, A. & Latora, V. Collective phenomena emerging from the interactions between dynamical processes in multiplex networks. *Phys. Rev. Lett.* **118**, 138302 (2017).
21. Danziger, M. M., Bonamassa, I., Boccaletti, S. & Havlin, S. Dynamic interdependence and competition in multilayer networks. *Nat. Phys.* **15**, 178–185 (2019).
22. Morris, R. G. & Barthelemy, M. Transport on coupled spatial networks. *Phys. Rev. Lett.* **109**, 128703 (2012).
23. Saito, Y., Nojima, T. & Iwasa, Y. Highly crystalline 2d superconductors. *Nat. Rev. Mater.* **2**, 16094 (2017).
24. Sacépé, B. et al. Localization of preformed cooper pairs in disordered superconductors. *Nat. Phys.* **7**, 239–244 (2011).
25. Doron, A., Levinson, T., Gorniaczyk, F., Tamir, I. & Shahar, D. The critical current of disordered superconductors near 0 K. *Nat. Commun.* **11**, 2667 (2020).
26. Parshani, R., Buldyrev, S. V. & Havlin, S. Interdependent networks: reducing the coupling strength leads to a change from a first to second order percolation transition. *Phys. Rev. Lett.* **105**, 048701 (2010).
27. Havlin, S. & Ben-Avraham, D. Diffusion in disordered media. *Adv. Phys.* **36**, 695–798 (1987).
28. Kirkpatrick, S. Percolation and conduction. *Rev. Mod. Phys.* **45**, 574–588 (1973).
29. Coniglio, A. Cluster structure near the percolation threshold. *J. Phys. A* **15**, 3829–3844 (1982).
30. Skvortsov, M. A. & Feigel'man, M. V. Superconductivity in disordered thin films: giant mesoscopic fluctuations. *Phys. Rev. Lett.* **95**, 057002 (2005).
31. Gurevich, A. V. I. & Mints, R. G. Self-heating in normal metals and superconductors. *Rev. Mod. Phys.* **59**, 941–999 (1987).
32. Danziger, M. M., Bashan, A. & Havlin, S. Interdependent resistor networks with process-based dependency. *New J. Phys.* **17**, 043046 (2015).
33. Bonamassa, I., Gross, B. & Havlin, S. Interdependent couplings map to thermal, higher-order interactions. Preprint at https://doi.org/10.48550/arXiv.2110.08907 (2021).
34. Cho, Y. S., Hwang, S., Herrmann, H. J. & Kahng, B. Avoiding a spanning cluster in percolation models. *Science* **339**, 1185–1187 (2013).
35. De Gennes, P.-G. On a relation between percolation theory and the elasticity of gels. *J. Physique Lett.* **37**, 1–2 (1976).
36. Ponta, L., Carbone, A., Gilli, M. & Mazzetti, P. Resistive transition in granular disordered high tc superconductors: a numerical study. *Phys. Rev. B* **79**, 134513 (2009).
37. Berman, R. The thermal conductivities of some dielectric solids at low temperatures (experimental). *Proc. R. Soc. Lond. Ser. A* **208**, 90–108 (1951).
38. Moore, A. L. & Shi, L. Emerging challenges and materials for thermal management of electronics. *Mater. Today* **17**, 163–174 (2014).
39. Binder, K. Theory of first-order phase transitions. *Rep. Prog. Phys.* **50**, 783–859 (1987).
40. Krzakala, F. & Zdeborová, L. On melting dynamics and the glass transition. i. glassy aspects of melting dynamics. *J. Chem. Phys.* **134**, 034512 (2011).
41. Zhou, D. et al. Simultaneous first-and second-order percolation transitions in interdependent networks. *Phys. Rev. E* **90**, 012803 (2014).
42. Zapperi, S., Lauritsen, K. B. & Stanley, H. E. Self-organized branching processes: mean-field theory for avalanches. *Phys. Rev. Lett.* **75**, 4071–4074 (1995).
43. Halperin, B. I. & Nelson, D. R. Theory of two-dimensional melting. *Phys. Rev. Lett.* **41**, 121–124 (1978).
44. Huang, B. et al. Layer-dependent ferromagnetism in a van der waals crystal down to the monolayer limit. *Nature* **546**, 270–273 (2017).
45. Gibertini, M., Koperski, M., Morpurgo, A. F. & Novoselov, K. S. Magnetic 2D materials and heterostructures. *Nat. Nanotechnol.* **14**, 408–419 (2019).

46. Shurakov, A., Lobanov, Y. & Goltsman, G. Superconducting hot-electron bolometer: from the discovery of hot-electron phenomena to practical applications. *Supercond. Sci. Technol.* **29**, 023001 (2015).
47. Meijer, G. I. Who wins the nonvolatile memory race? *Science* **319**, 1625–1626 (2008).

Methods

Sample preparation

The interdependent superconducting system (see the schematic representation in Fig. 1b, main text) was prepared as follows. (i) On a (Si/SiO_2) substrate we electron-beam evaporated a thin film of 50 nm a:InO with partial oxygen pressure (6–8 μTorr), resulting in a disordered superconductor with a bulk critical temperature $T_c \approx 3$ K. The layer was patterned to form a network consisting of 31 × 31 stripes, each one being 4 μm wide and 720 μm long (Fig. 1b, inset), thus resulting in a superconducting lattice composed of segments with dimensions $4 \times 20\ \mu m^2$ and height $h \approx 50$ nm. (ii) For the electrically insulating medium, we evaporated a thin film of 100–150 nm of Al_2O_3 on top of the network at high partial O_2 pressure in order to achieve a pinhole-free film. (iii) On the top of the Al_2O_3 layer, we evaporated a second superconducting network sample, perfectly overlapping the first one (Fig. 1b, inset). (iv) We then fabricated two Au contacts of 4-nm-thick Cr + 35 nm Au at the edges of each network in order to enable independent transport measurements. The adoption of Al_2O_3 as a coupling medium is motivated by its strong electrical insulating properties and relatively large thermal conductivity ($\kappa_{Al_2O_3} \approx 10\ W\ m^{-1}\ K^{-1}$ at $T \approx 3$ K, from ref. 37), which enables the realization of cross-layer heat transfer without the hopping of electrons.

Measurements

We performed d.c. transport measurement using a Keithley 2410 sourcemeter and a Keithley 2000 multimeter for each network. The cryostat temperature was tuned via a LakeShore 330 using a 25 Ω heater and a DT-670 thermometer was placed inside the cryostat. We started by measuring the global sheet resistance of each superconducting array with adiabatic heating–cooling cycles in the temperature range base to 10 K for different values of the driving current, I_b. After characterizing the phase diagrams of each isolated array (Fig. 4b, inset), we checked the absence of shorts between the layers by measuring the junction resistance between each pair of cross contacts. The cross-layer couplings are created by passing the same current within both layers simultaneously, thus generating dependency links sustained by heat transfer. D.c. transport measurements were then performed in the thermally interdependent setup with adiabatic heating–cooling cycles for the same currents as in the isolated case, yielding the curves in Fig. 1f and the coupled phase diagram in Fig. 4b.

RSJJ model of disordered superconductors

To characterize the SN transitions observed in the experiments, we model each disordered superconductor via a disordered 2D lattice of RSJJs. Isolated networks of RSJJs undergo continuous SN phase transitions at low temperatures that, in the limit of large tunnelling conductances (that is, $g \gg 1$), are generally independent of the ratio between the Josephson E_J and the Coulomb E_C energies[48–50]. In this regime, each junction's state can be characterized by the value of its normal-state resistance, $R_n(T)$, and by its critical current, $I_c(T)$, which generally depend on the ratio between the temperature T of the cryostat and the junction's SN activation threshold T_c. When dealing with ordered superconducting arrays, the letter quantities satisfy in the so-called dirty limit[51,52] the Ambegaoakar–Baratoff relation[53,54] $I_c(T)R_n = \frac{\pi}{2e}\Delta(T)\tanh(\Delta(T)/2k_BT)$, where the energy gap, $\Delta(T)$, follows the Bardeen–Cooper–Schrieffer mean-field spectral relation $2\Delta(T) \approx \alpha k_B T_c$ with $\alpha \approx 3.53$. In the previous relations, k_B is the Boltzmann constant and e is the elementary charge. In disordered superconductors, on the other hand, disorder-induced spatial inhomogeneities of the SC state break the ideal Bardeen–Cooper–Schrieffer scheme in the above, yielding striking phenomena[55] such as non-monotonic variations of the sheet resistance[56], suppression of T_c towards zero[57] and large values[24] of the spectral gap ratio $\Delta(T)/T_c$. When modelling these networks via RSJJs, an Arrhenius activation law at low temperatures[58] is invoked to include the presence of large resistive areas due to the emergence of insulating islands. The a:InO samples fabricated in the present work, however, have bulk SN thresholds large enough to ensure that junctions rarely undergo a metal–insulator transition. In light of this, we consider a model of RSJJ with only three electronic states: superconducting (SC), intermediate (IM) and normal metal (N), defined according to the Josephson I–V characteristic displayed in Fig. 2b. Hence, the junction's resistance is defined piecewise as:

$$R_{ij} = \begin{cases} R_\epsilon, & \text{if } V_{ij} < R_\epsilon I_{ij}^c(T)\text{(SC)}, \\ R_{ij}^n, & \text{if } V_{ij} > R_{ij}^n I_{ij}^c(T)\text{(N)}, \\ V_{ij}/I_{ij}^c(T), & \text{otherwise (IM)}, \end{cases} \quad \text{(M1)}$$

where R_ϵ is the resistance in the SC state ($R_\epsilon = 10^{-5}\,\Omega$ in the simulations, see equation (M4) for details) and V_{ij} is the potential drop measured at the junction's ends. For the critical currents, we propose a local generalization of the de Gennes relation, that is equation (1), where $I_{ij}^c(0)$ is the junction's critical current at $T = 0$. We control the degree of disorder in the arrays by considering a quenched normal distribution $\chi_{ij} \in \mathcal{N}(0,\sigma)$ —where variables match the junctions' labels in each array—with zero mean and variance σ as a generator for the other system's observables. In particular, we define $I_{ij}^c(0) = I_0^c(1+\chi_{ij})$, $T_{ij}^c = T_c(1+\chi_{ij})$ and $R_{ij}^n = \rho R_q(1+\chi_{ij})$, where $R_q \approx 6.45\ k\Omega$ is the quantum resistance for pairs, so that junctions with a large zero-T threshold have a comparably large critical temperature and normal resistance. The values of I_0^c, T_c and ρ can be extrapolated from the experimental data; T_c, in particular, can be found by fitting to the resistive curves the Aslamazov–Larkin correction[59,60] or, similarly, the HN relation[61] adopted in the main text. Best fitted values for I_0^c, T_c and ρ are listed in the caption to Fig. 2.

Thermally coupled Kirchhoff equations

To characterize the mutual SN phase transitions reported in the experiments, we have developed a model of thermally coupled RSJJs networks with local thermal couplings sustained by the heat dissipation of single junctions. Alike simulations in interdependent networks[62], numerical solutions for the mutual order parameter (here, the global sheet resistance, R) can be obtained recursively by making the layers to adaptively interact through their isolated behaviours[36]. In our model of thermally interdependent RSJJ networks, this is achieved by solving the Kirchhoff equations of each array under the adaptive effect set by the 'two-interaction' interplay between equation (1) and equation (2). We consider therefore two layers, A and B, each being a 2D lattices with linear size L, whose left and right boundaries are connected to an external supernode (source) where the bias current is injected and to the ground, respectively. Each junction has a Josephson I–V characteristic with R_{ij} defined as in equation (M1), where we assume $R_\epsilon = 10^{-5}\,\Omega$ for both the arrays and mean normal resistance $R_n = \rho R_q$, with $\rho_A = 1.24$ and $\rho_B = 0.77$. We initiate the algorithm by randomly assigning two vector potentials $\mathbf{V}_\mu$ with $\mu = A, B$ with same values for all junctions at the zeroth iteration. When starting from the mutual SC state, the junctions' resistances in both layers are set as $R_{ij}^A = R_{ij}^B = R_\epsilon$, whilst $R_{ij}^A = R_{ij,A}^n$ and $R_{ij}^B = R_{ij,B}^n$ when the layers start from their mutual N phase. The algorithm evolves iteratively as follows:

(1) at the t-th stage ($t \geq 1$) of the overheating cascade, the local effective temperatures, equation (2), are computed using the resistances and the local currents found at the stage ($t-1$);
(2) the critical currents $I_{ij}^c(T)$ are updated via equation (1), and their resistive state is determined via equation (M1) after computing the potential drop $V_{ij,t}$ from the vector $\mathbf{V}_t$;
(3) the (symmetric) conductance matrices $\tilde{G}_\mu$ with $\mu = A, B$ are generated via the junctions' resistances in (2) with entries

$$G_{ij} = \begin{cases} 0, & \text{if } (i,j) \notin E \\ -1/R_{ij}, & \text{if } (i,j) \in E \\ \sum_{k\in\partial i} 1/R_{ik}, & \text{if } i = j \end{cases} \quad \text{(M2)}$$

where E is the set of edges in each array and ∂i the set of nearest neighbours of node i;

(4) the potential vectors, $\mathbf{V}_{\mu,t+1}$, are updated by solving numerically the Kirchhoff matrix equations

$$\begin{cases} \bar{G}_t^A \cdot \mathbf{V}_{t+1}^A = \mathbf{I}_{\text{inj}}^A \\ \bar{G}_t^B \cdot \mathbf{V}_{t+1}^B = \mathbf{I}_{\text{inj}}^B \end{cases} \tag{M3}$$

where $(\cdot)$ is the matrix product and $\mathbf{I}_{\text{inj}}^{\mu}$ is the vector of total currents injected to each node at every stage, whose elements are always zeroes except for the first entry (the supernode) which equals the driving current I_{b}^{μ} with $\mu = A, B$;

(5) the global sheet resistances of each array are then calculated as $R_{t+1}^{\mu} = \mathbf{W}_{t+1}^{\mu}/I_{\text{b}}^{\mu}$ with $\mu = A, B$.

The steps (1)–(5) are recursively repeated yielding a sequence of pairs of vector potentials: $\{(\mathbf{W}_0^{\mu}, \mathbf{W}_0^{B}), \ldots, (\mathbf{W}_t^{A}, \mathbf{W}_t^{B}), \ldots\}$, whose convergence is verified as soon as the mutual error

$$\delta\mathbf{W} = \sum_{\mu=A,B} \left| 1 - \frac{\mathbf{W}_t^{\mu}}{\mathbf{W}_{t+1}^{\mu}} \right|$$

becomes smaller than a numerical precision ε_{min}. In the simulations carried on in the present work, we used $\varepsilon_{\text{min}} = 10^{-5}$ although we verified that higher precision thresholds do not alter the phase diagram of decoupled and thermally interdependent networks.

Let us notice that, in the above, each pair of superposed junctions in the two RSJJ networks is assumed to be one-to-one thermally coupled. This is because, in our model, the strength of dependency couplings can be controlled via the amount of power dissipated by Joule heating, that is by the amount of bias current, I_{b}, pumped in the system. From the viewpoint of interdependent network theory, this realizes the model of partial interdependent networks and an increase in the levels of I_{b} would correspond to an increase of the fraction[17] of interdependent pairs between the layers. In this respect, an increase of the thickness of the Al_2O_3 medium of our experiment would have the equivalent effect of reducing the strength of the dependency couplings between the layers.

Thermal dependency between layers

Equation (2) approximates the local overheating of the junction (i,j) in a given layer due to the thermal heat transferred from its superposed junction in the other layer. To obtain equation (2), let us study the more general case where the junction (i,j) in layer $\mu = A, B$ is also overheated by its $\partial(i,j)$ neighbouring junctions. In such a case, we can compute T_{ij}^{μ} by resorting to the thermal analogue of circuit theory. With reference to the illustration in Supplementary Fig. 8, let us consider the overheating of the junction (i,j) in layer B. The total heat flowing towards (i,j) in layer B, $\dot{Q}_{ij}^{B}$, can be approximated as the sum of two parallel paths: the heat dissipated by the overlapping junction (i,j) in layer A and transferred through the coupling medium, and the heat reaching (i,j) of B from its six nearest neighbours, namely

$$\dot{Q}_{ij}^{B} = \dot{Q}_{ij}^{B\leftarrow A} + \dot{Q}_{\partial(i,j)}^{B\leftarrow B}.$$

Each contribution to the heat flow can be written in terms of the (total) thermal conductance, γ, of the corresponding medium. In particular, one finds that $\dot{Q}_{ij}^{B\leftarrow A} = \gamma_{AB}(T_{ij}^{B} - T)$ and

$$\dot{Q}_{\partial(i,j)}^{B\leftarrow B} = (T_{ij}^{B} - T) \sum_{k\in\partial(i,j)} \gamma_k^{B} = 6\gamma_B(T_{ij}^{B} - T),$$

where, for the last identity, we noticed that the neighbours of (i,j) in layer B are, themselves, in a thermal parallel and that, by geometry, they all have the same thermal conductance, γ_B. Combining the above, we get $\dot{Q}_{ij}^{B} = \gamma_{\text{eq}}^{B}(T_{ij}^{B} - T)$, where $\gamma_{\text{eq}}^{B} \equiv \gamma_{AB} + 6\gamma_B$. Equivalent arguments yield the analogous expression for layer A, that is $\dot{Q}_{ij}^{A} = \gamma_{\text{eq}}^{A}(T_{ij}^{A} - T)$, where now $\gamma_{\text{eq}}^{A} = \gamma_{AB} + 6\gamma_A$.

The values of γ_{eq}^{μ} characterizing our experimental setup can be calculated via $\gamma = \kappa\mathcal{A}/\ell$, where κ is the thermal conductivity of the medium, $\mathcal{A}$ the cross-sectional area where heat flows and ℓ its thickness. For our samples (see equation (1) for details), we have $\kappa_{SiO_2} = 0.2\,\text{W m}^{-1}\,\text{K}^{-1}$ and $\kappa_{Al_2O_3} = 10\,\text{W m}^{-1}\,\text{K}^{-1}$, so that

$$\gamma_{AB} = 8 \times 10^{-3}\ \text{W K}^{-1},$$
$$\gamma_{SiO_2} = 5 \times 10^{-9}\ \text{W K}^{-1},$$
$$\gamma_{Al_2O_3} = 2.5 \times 10^{-7}\ \text{W K}^{-1}.$$

Since layer A (top layer) is deposited over the Al_2O_3 medium, while layer B (bottom layer) is roughly embedded for half of its width in the underlying SiO_2 substrate (Fig. 1b), we have that $\gamma_{\text{eq}}^{A} = \gamma_{AB} + 6\gamma_{Al_2O_3}$ and $\gamma_{\text{eq}}^{B} = \gamma_{AB} + 6\left(\gamma_{SiO_2} + \gamma_{Al_2O_3}\right)$. Hence, because the thickness of the Al_2O_3 coupling medium is roughly two orders of magnitude (Fig. 1b, inset) smaller then the average lattice spacing within each array, we have that $\gamma_{\text{eq}}^{\mu} \approx \gamma_{AB}$ for $\mu = A, B$, that is, the heat is mainly dissipated between the layers or, equivalently, thermal interdependence is negligible within the layers.

To arrive at equation (2), it is sufficient to notice that the heat rate, $\dot{Q}$, is actually proportional to the power, $\mathcal{P}_{ij} = R_{ij}^{A} I_{ij,A}^{2}$, dissipated by Joule heating in the corresponding resistors, where I_{ij} is the current flowing through the junction (i,j) whose electrical resistance is R_{ij}. Therefore, to compare $\dot{Q}$ with $\mathcal{P}$, one has to consider the different time scales characterizing these energy rates: while the former is given by the characteristic time, τ_{p}, of thermal conduction through a given medium, the latter is expressed instead in units of the characteristic time, τ_{e}, needed by the current flowing in the circuit to reach a steady distribution. This leads to the relation $\dot{Q} = \tau_{\text{p}}/\tau_{\text{e}}\mathcal{P}$. Combining the above expressions for $\dot{Q}_{ij}^{B}$, we get equation (2) in the main text. The characteristic time τ_{e} to reach equilibration in the current distribution can be estimated via the time needed by electrons to span the linear size of the superconducting arrays, that is $L = 620\,\mu\text{m}$, namely $\tau_{\text{e}} = cL \approx 2 \times 10^{-12}\,\text{s}$, where $c \approx 2.99 \times 10^{8}\,\text{m s}^{-2}$ is the speed of light. The characteristic time of thermal conduction can be estimated instead as the time needed for heat to flow through a medium of density $\tilde{\eta}$ and thickness ℓ, whose expression[63] is given by $\tau_{\text{p}} = C\tilde{\eta}\ell^2/\kappa$, where C is the material's specific heat. Since $C_{Al_2O_3} \approx 880\,\text{J kg}^{-1}\,\text{K}^{-1}$ and $\tilde{\eta}_{Al_2O_3} \approx 3.89\,\text{g cm}^{-3}$, we find that $\tau_{\text{p}} \approx 3.4 \times 10^{-6}\,\text{s}$ and, therefore, $\tau_{\text{p}}/\tau_{\text{e}} \approx 1.7 \times 10^{6}$.

Validity of the mean-field hypothesis

Non-locality is essential for the large-scale propagation of cascades[64]. In our model of thermally interdependent 2D SC networks, the random redistribution of the currents after the state switch of single junctions non-locally propagates local phase perturbations, setting an effective long-range feedback within each layer. Recent findings on percolation in interdependent spatial networks[65–67] show that randomly interdependent lattices (that is, coupled 2D grids with long-range dependency links) and multiplex disordered lattices (that is, coupled spatially embedded networks with long-range connectivity links and dependency links between overlapping nodes) are physically equivalent, featuring qualitatively similar equilibrium phases and dynamical regimes. This equivalence finds solid grounds in the mapping[33] we have recently discovered between percolation in $K > 2$ randomly interdependent networks and the onset of hard fields in the one-step replica-symmetry-breaking solution of the random $(K+1)$-XORSAT problem[33,68], that is, with the ground state of ferromagnetic $(K+1)$-spin models on random hypergraphs. Since an interdependent link between nodes interacting with their nearest neighbours via pairwise couplings maps exactly onto a hyperedge made by triads of the two dependent

nodes and their nearest neighbours, a source of long-rangedness either on the dependency links or on the connectivity links yields statistically equivalent structures (that is, hypergraphs with triads between two nodes at short-range distance and one randomly chosen node within the arrays). In light of this, the mean-field hypothesis advanced in the main text can be read as the completely random version of the above, which does not alter the main phenomenology of first-order transitions and the cascade of failures observed in fully random interdependent networks[62].

Data availability

Source data are provided with this paper. All data supporting our findings are available from the corresponding author upon reasonable request.

Code availability

Source codes and videos showing the states of resistors, their currents and the power dissipated in both layers during the transition can be freely accessed at the GitHub repository: https://github.com/BnayaGross/Interdependent-SC-networks.

References

48. Orr, B. G., Jaeger, H. M., Goldman, A. M. & Kuper, C. G. Global phase coherence in two-dimensional granular superconductors. *Phys. Rev. Lett.* **56**, 378–381 (1986).
49. Chakravarty, S., Ingold, G.-L., Kivelson, S. & Luther, A. Onset of global phase coherence in josephson-junction arrays: a dissipative phase transition. *Phys. Rev. Lett.* **56**, 2303–2306 (1986).
50. Chakravarty, S., Ingold, G.-L., Kivelson, S. & Zimanyi, G. Quantum statistical mechanics of an array of resistively shunted josephson junctions. *Phys. Rev. B* **37**, 3283–3294 (1988).
51. Abraham, D. W., Lobb, C. J., Tinkham, M. & Klapwijk, T. M. Resistive transition in two-dimensional arrays of superconducting weak links. *Phys. Rev. B* **26**, 5268–5271 (1982).
52. Lobb, C. J., Abraham, D. W. & Tinkham, M. Theoretical interpretation of resistive transition data from arrays of superconducting weak links. *Phys. Rev. B* **27**, 150–157 (1983).
53. Josephson, B. D. Possible new effects in superconductive tunnelling. *Phys. Lett.* **1**, 251–253 (1962).
54. Ambegaokar, V. & Baratoff, A. Tunnelling between superconductors. *Phys. Rev. Lett.* **10**, 486–489 (1963).
55. Dubi, Y., Meir, Y. & Avishai, Y. Nature of the superconductor-insulator transition in disordered superconductors. *Nature* **449**, 876–880 (2007).
56. Baturina, T. I., Mironov, A. Y., Vinokur, V. M., Baklanov, M. R. & Strunk, C. Localized superconductivity in the quantum-critical region of the disorder-driven superconductor-insulator transition in tin thin films. *Phys. Rev. Lett.* **99**, 257003 (2007).
57. Sacépé, B. et al. Disorder-induced inhomogeneities of the superconducting state close to the superconductor-insulator transition. *Phys. Rev. Lett.* **101**, 157006 (2008).
58. Ponta, L., Andreoli, V. & Carbone, A. Superconducting-insulator transition in disordered josephson junctions networks. *Eur. Phys. J. B* **86**, 1–5 (2013).
59. Aslamazov, L. G. & Larkin, A. I. in *30 Years Of The Landau Institute* Vol. 11 (ed. Khalatnikov, I. M.) 23–28 (World Scientific Series in 20th Century Physics, 1996).
60. Baturina, T. I. et al. Superconductivity on the localization threshold and magnetic-field-tuned superconductor-insulator transition in tin films. *J. Exp. Theor. Phys. Lett.* **79**, 337–341 (2004).
61. Halperin, B. I. & Nelson, D. R. Resistive transition in superconducting films. *J. Low Temp. Phys.* **36**, 599–616 (1979).
62. Gao, J., Buldyrev, S. V., Stanley, H. E. & Havlin, S. Networks formed from interdependent networks. *Nat. Phys.* **8**, 40–48 (2012).
63. Rowe, D. M. *Thermoelectrics Handbook: Macro to Nano* (CRC Press, 2018).
64. Motter, A. E. & Yang, Y. The unfolding and control of network cascades. *Phys. Today* **70**, 32–39 (2017).
65. Li, W., Bashan, A., Buldyrev, S. V., Stanley, H. E. & Havlin, S. Cascading failures in interdependent lattice networks: the critical role of the length of dependency links. *Phys. Rev. Lett.* **108**, 228702 (2012).
66. Danziger, M. M., Shekhtman, L. M., Berezin, Y. & Havlin, S. The effect of spatiality on multiplex networks. *Europhys. Lett.* **115**, 36002 (2016).
67. Gross, B., Bonamassa, I. & Havlin, S. Interdependent transport via percolation backbones in spatial networks. *Physica A* **567**, 125644 (2021).
68. Mezard, M. & Montanari, A. *Information, Physics, and Computation* (Oxford Univ. Press, 2009).

Acknowledgements

S.H. acknowledges financial support from the Israel Science Foundation (ISF), the China–Israel Science Foundation, the Office of Naval Research (ONR), the Bar-Ilan University Center for Research in Applied Cryptography and Cyber Security, the EU project RISE, the US-Israel Binational Science Foundation (NSF-BSF) grant no. 2019740 and the Defense Threat Reduction Agency (DTRA) grant no. HDTRA-1-19-1-0016. I.B., A.F. and S.H. acknowledge partial support from the Italy-Israel grant 'EXPLICS'. A.F. acknowledges partial support from the ISF Israel–China grant no. 3192/19. B.G. acknowledges the support of the Mordecai and Monique Katz Graduate Fellowship Program. We thank A. Bashan, M. M. Danziger and S. Boccaletti for stimulating discussions.

Author contributions

I.B., A.F. and S.H. initiated and designed the research. M.L., I.V. and A.F. fabricated the samples, carried on the experiments and collected the data. I.B. and B.G. developed the modelling and the adaptive algorithm for solving the thermally coupled Kirchhoff equations. B.G. designed the codes. B.G. and I.B. carried out the numerical simulations. I.B. designed and created the figures. I.B. developed the mean-field theory. I.B. was the leading writer of the paper with contributions from B.G., S.H. and A.F. A.F. and S.H. supervised the research. All authors critically reviewed and approved the paper.

Competing interests

The authors declare no competing interests.

Additional information

Supplementary information The online version contains supplementary material available at https://doi.org/10.1038/s41567-023-02029-z.

Correspondence and requests for materials should be addressed to I. Bonamassa.

Peer review information *Nature Physics* thanks Juan Rocha, Simon Levin and the other, anonymous, reviewer(s) for their contribution to the peer review of this work.